Experiments and simulations of a magnetic arch plasma expansion for space propulsion

(P. Jiménez)
M. Merino, C. Boyé, D. García-Lahuerta, J. Navarro-Cavallé, E. Ahedo
Equipo de Propulsión Espacial y Plasmas (EP2),
Universidad Carlos III de Madrid, Leganés, Spain

ICOPS 2023

Contents

- Electrodeless plasma thrusters in tandem; “magnetic arch” plasma expansion
- Collisionless, quasineutral, two-fluid model of the magnetic arch plasma expansion
- Simulation results of the plasma expansion (2D planar)
  - Electron, ion properties
  - Electric currents and magnetic thrust generation
  - Plasma-induced magnetic field
- Laboratory setup with two ECR plasma sources firing in parallel
- Experimental results
  - Ion current density (FC)
  - Ion energy (RPA)
- Conclusions

Electrodeless plasma thrusters, in tandem

- Existing electrodeless plasma thrusters (EPTs) feature a discharge chamber and a magnetic nozzle
  - Single sources have a strong magnetic dipole that, in orbit, would cause a secular magnetic torque when interacting with the geomagnetic field
- Simple solution: fly EPTs in tandem, with opposing polarities
  - This also offers the opportunity of thrust vector control
- The connecting lines of the two magnetic nozzles generate a new topology: the magnetic arch
  - Question: will the plasma expand and form a beam in spite of the closed magnetic lines?
- Secondary motivation: new thruster geometries also feature a magnetic arch, like the C-thruster:
  - Avoids rear walls of cylindrical sources; tangential $\boldsymbol{B}$ field shield all internal walls

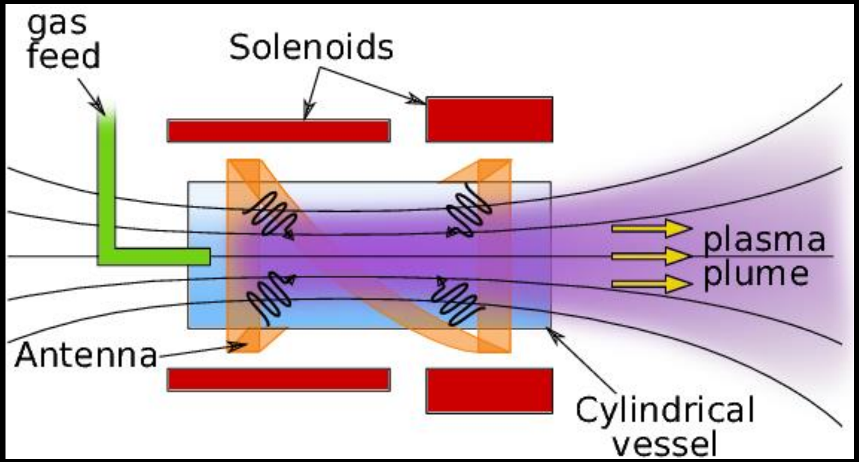

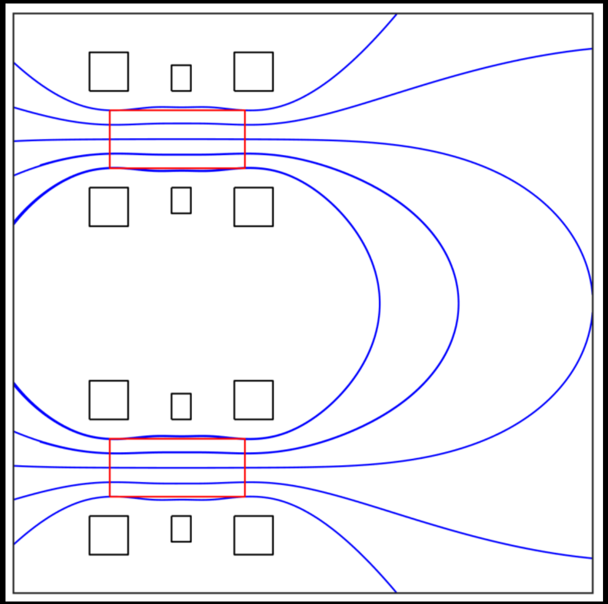

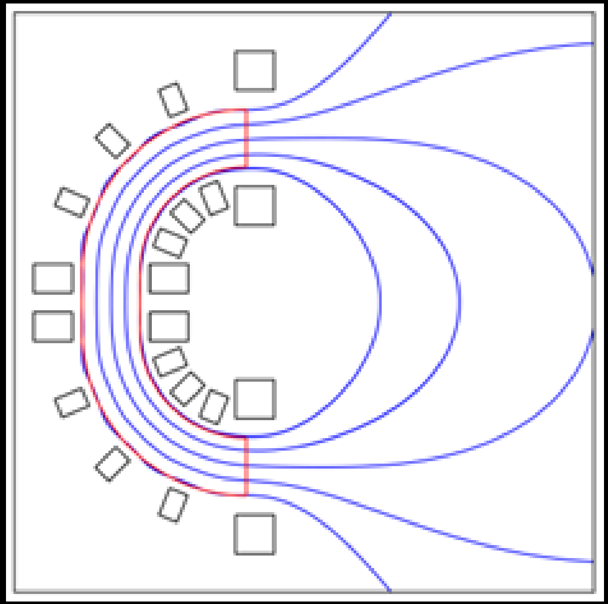

Magnetic Arch plasma model

- Quasineutral, collisionless, two-fluid (ions, electrons)
- 2D planar (future work must deal with full 3D case)
- Applied magnetic field admits streamfunction ψ_B:

$$\frac{\partial \psi_B}{\partial z} = -B_x \qquad \frac{\partial \psi_B}{\partial x} = B_z$$

  - Red streamline separates "inner" (connected) and "outer" magnetic lines
- Fluid equations of massless, fully-magnetized, polytropic electrons and cold ions (all dimensionless):

$$\frac{\partial n}{\partial t} + \nabla \cdot (n\boldsymbol{u}_e) = 0,$$
$$0 = -\nabla(nT_e) + n\nabla\phi - n\boldsymbol{u}_e \times \boldsymbol{B},$$
$$\frac{\partial n}{\partial t} + \nabla \cdot (n\boldsymbol{u}_i) = 0,$$
$$\frac{\partial n\boldsymbol{u}_i}{\partial t} + \nabla \cdot (n\boldsymbol{u}_i\boldsymbol{u}_i) = -n\nabla\phi + n\boldsymbol{u}_i \times \boldsymbol{B}.$$

$$n \equiv n_e = n_i$$
$$T_e = n^{\gamma-1}$$

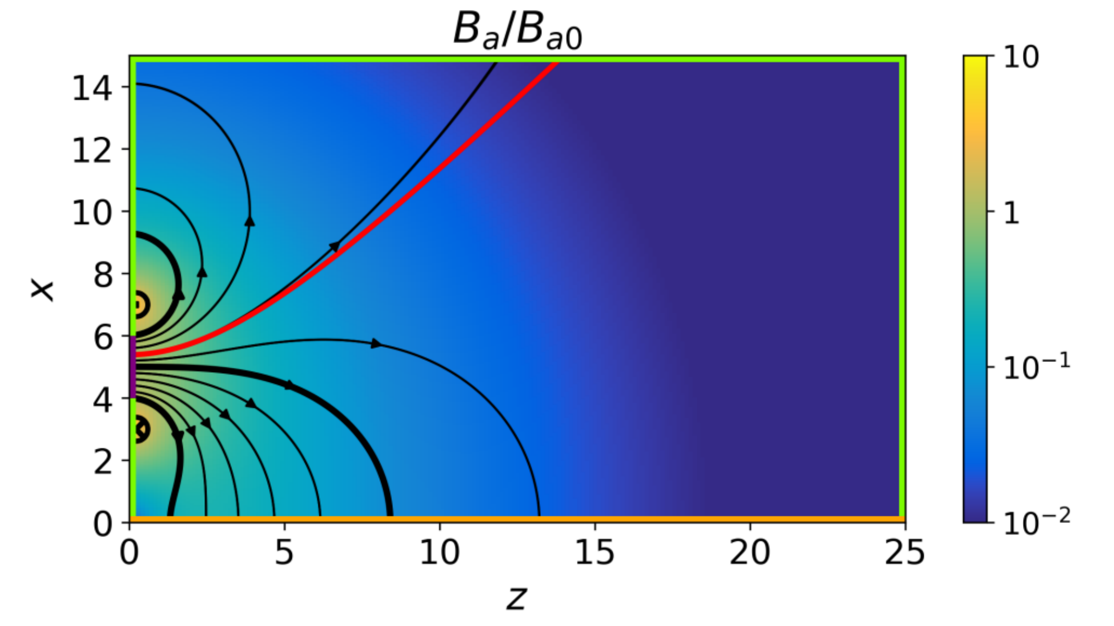

- Simulation domain exploits symmetry plane
- Injection of known plasma profile on the left (Gaussian n, sonic ions)
- Free outflow boundaries elsewhere

Electron model

- Electron momentum equation reduces to:

$$0 = -\nabla\left(\frac{\gamma}{\gamma-1}n^{\gamma-1} - \phi\right) - u_{ye}B\mathbf{1}_\perp$$

- This yields the following energy conservation law in the parallel direction (H_e is a function of the magnetic streamline):

$$H_e(\psi_B) = \frac{\gamma}{\gamma-1}\left[n^{\gamma-1} - 1\right] - \phi,$$

- Perpendicular equation yields the out-of-plane electron velocity, which plays a central role in magnetic thrust generation:

$$u_{ye}(\psi_B) = -\frac{1}{B}\frac{\partial H_e}{\partial \mathbf{1}_\perp} = -\frac{\mathrm{d}H_e}{\mathrm{d}\psi_B}$$

- Continuity equation yields $u_{\parallel e}$ a posteriori: $$\frac{\partial n u_{\parallel e}/B}{\partial \mathbf{1}_b} = 0$$

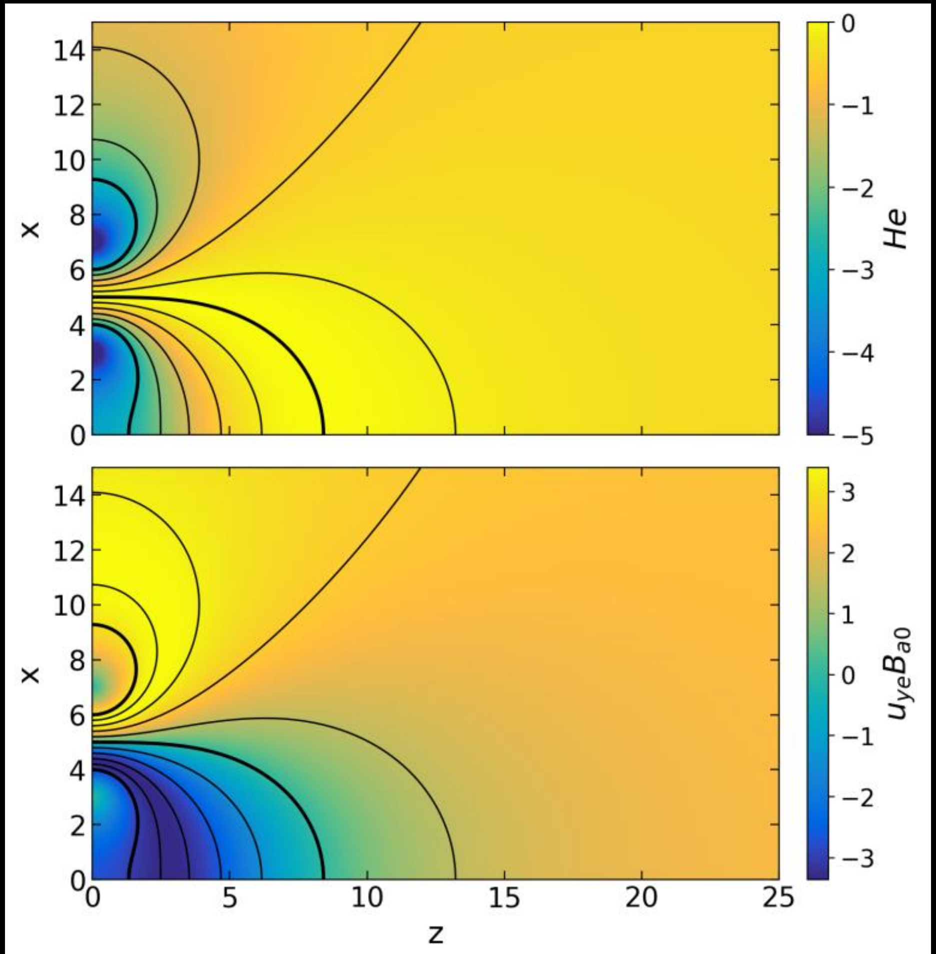

Ion model

- After substituting ϕ from $\phi(n,\psi_B) = \frac{\gamma}{\gamma-1}[n^{\gamma-1}-1] - H_e(\psi_B)$

  the ion equations read as follows and are integrated with a discontinuous Galerkin (1st order elements) until steady state:

$$\frac{\partial n}{\partial t} + \frac{\partial n u_{zi}}{\partial z} + \frac{\partial n u_{xi}}{\partial x} = 0$$

$$\frac{\partial n u_{zi}}{\partial t} + \frac{\partial n u_{zi} u_{zi}}{\partial z} + \frac{\partial n u_{xi} u_{zi}}{\partial x} + \frac{\partial n^\gamma}{\partial z} = -n\left(\frac{\partial H_e}{\partial \psi_B} + u_{yi}\right) B_x,$$

$$\frac{\partial n u_{xi}}{\partial t} + \frac{\partial n u_{xi} u_{zi}}{\partial z} + \frac{\partial n u_{xi} u_{xi}}{\partial x} + \frac{\partial n^\gamma}{\partial x} = n\left(\frac{\partial H_e}{\partial \psi_B} + u_{yi}\right) B_z,$$

$$\frac{\partial n u_{yi}}{\partial t} + \frac{\partial n u_{yi} u_{zi}}{\partial z} + \frac{\partial n u_{xi} u_{yi}}{\partial x} = n(u_{zi}B_x - u_{xi}B_z),$$

  - Ions initially accelerate as in a simple magnetic nozzle
  - Oblique shock structure forms where ions from the two thruster outlets interact (at the symmetry plane).
  - Ion jet is able to propagate beyond the closed magnetic tube, in spite of closed magnetic lines

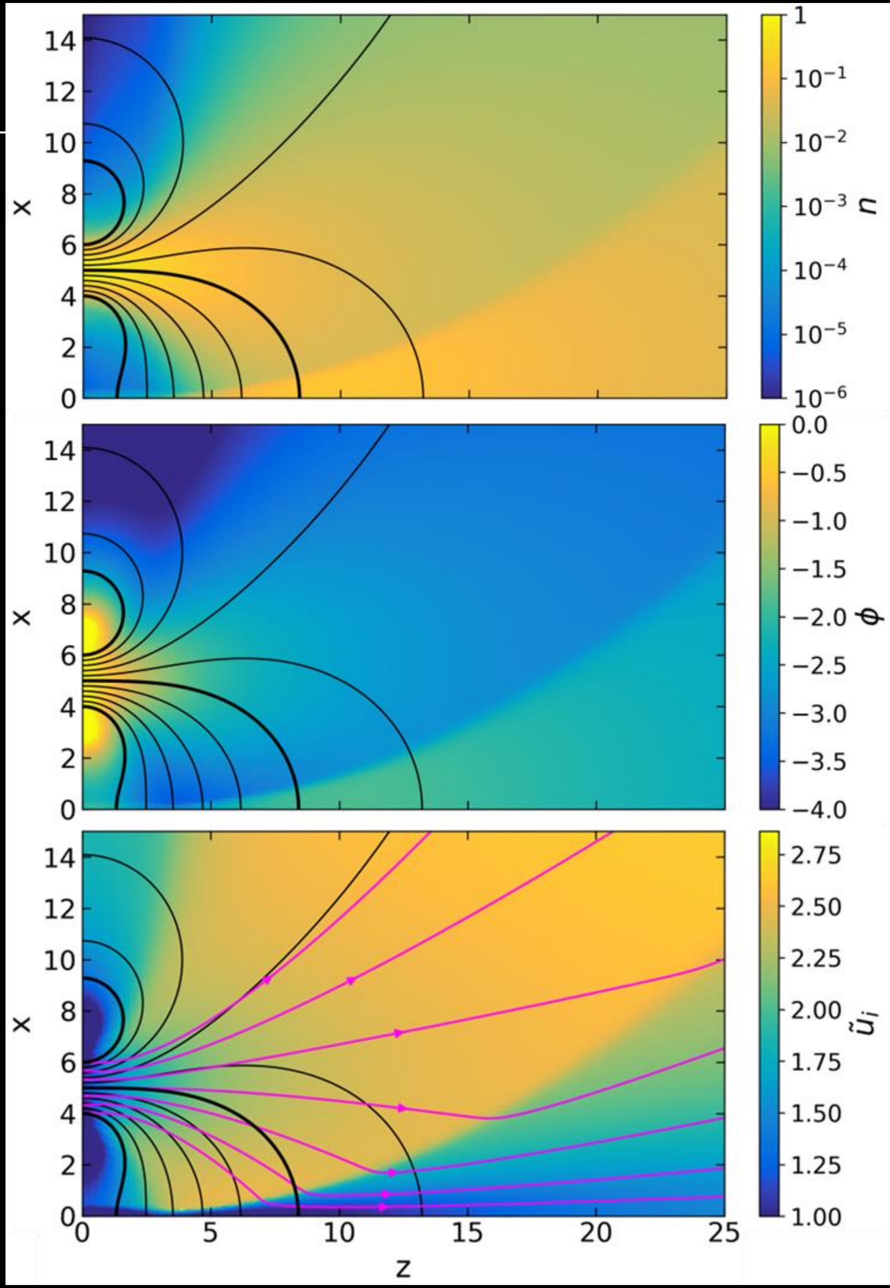

Magnetic force density and magnetic thrust

- Electron out-of-plane current density dominates and determines magnetic force on the plasma

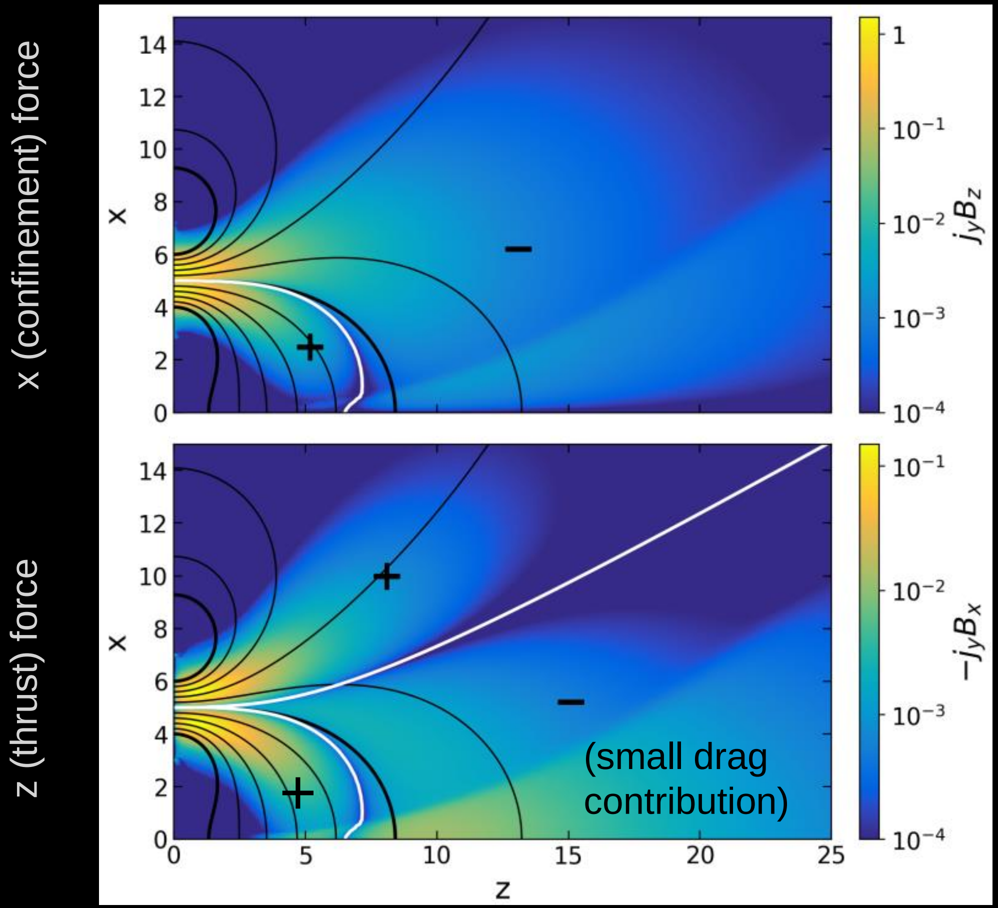

- Integrated magnetic thrust force up to $z = \mathrm{const}$ shows that net increase in thrust is achieved by the magnetic arch
  - Small drag contribution where plasma crossed the closed magnetic lines

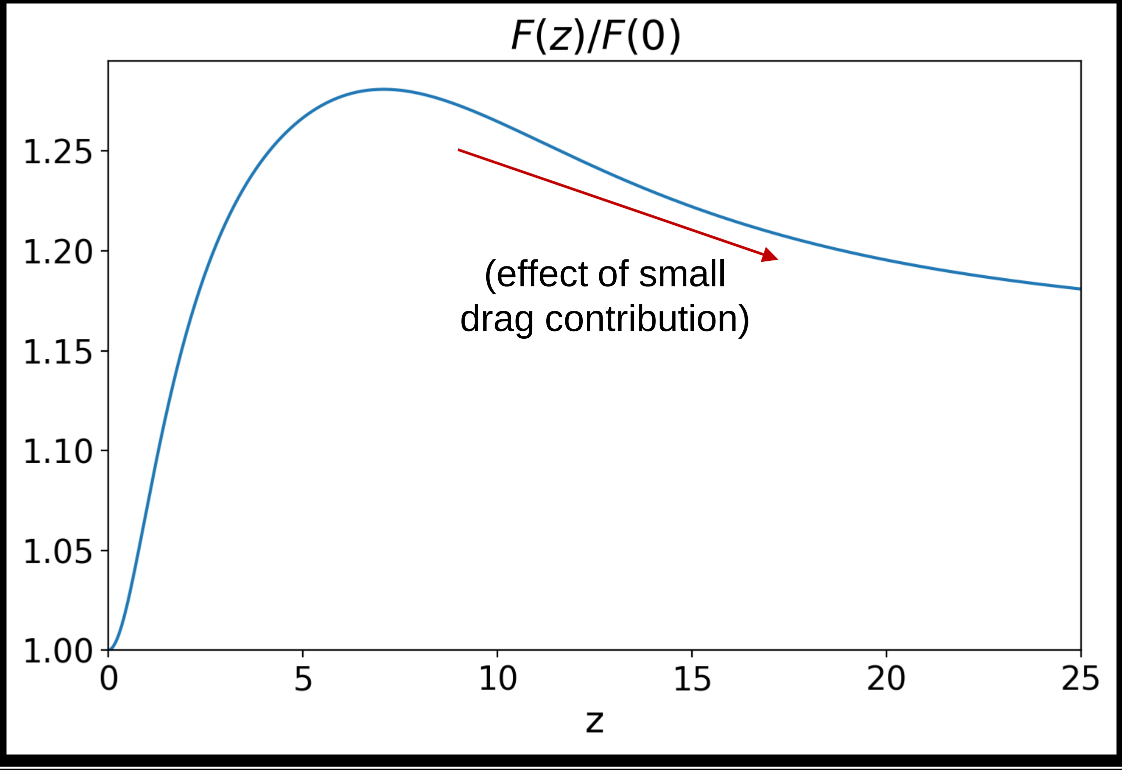

Plasma-induced magnetic field

- Out-of-plane j_y currents generate plasma-induced field $\boldsymbol{B}_p$. The relative importance B_p/B_a increases with $\beta_0 = \mu_0 n_0 T_0 / B_{a0}^2$
- Induced field stretches total field downstream, elongating the magnetic arch
- For high enough β_0, new magnetic region (disconnected from source) forms

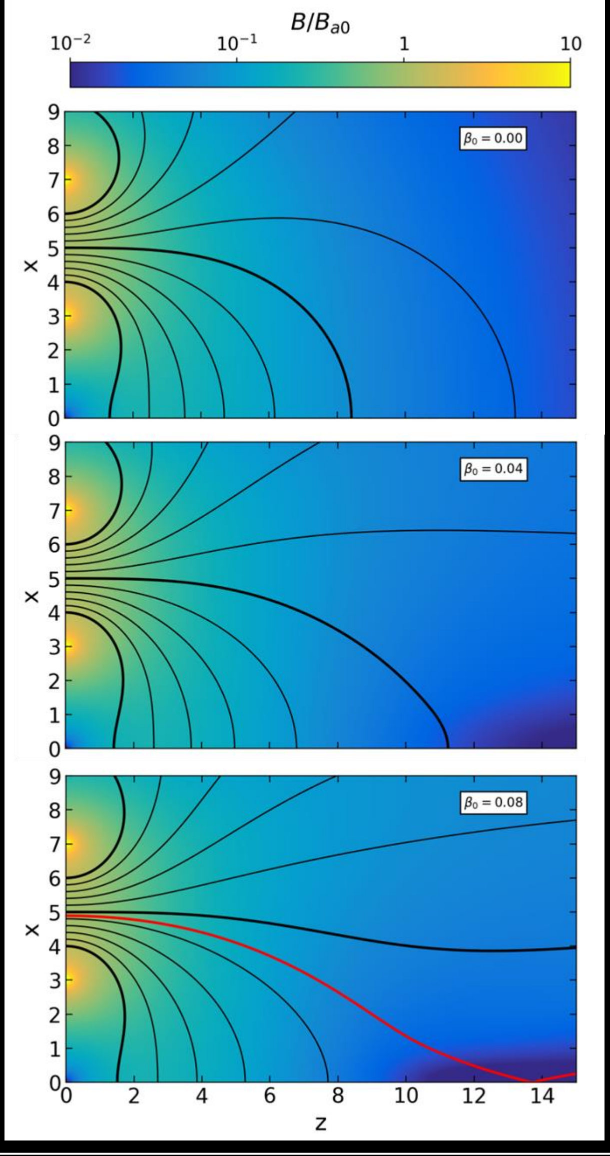

- The plasma induced magnetic field changes the generated magnetic thrust
- Higher values of β_0 result in higher, monotonic thrust curve

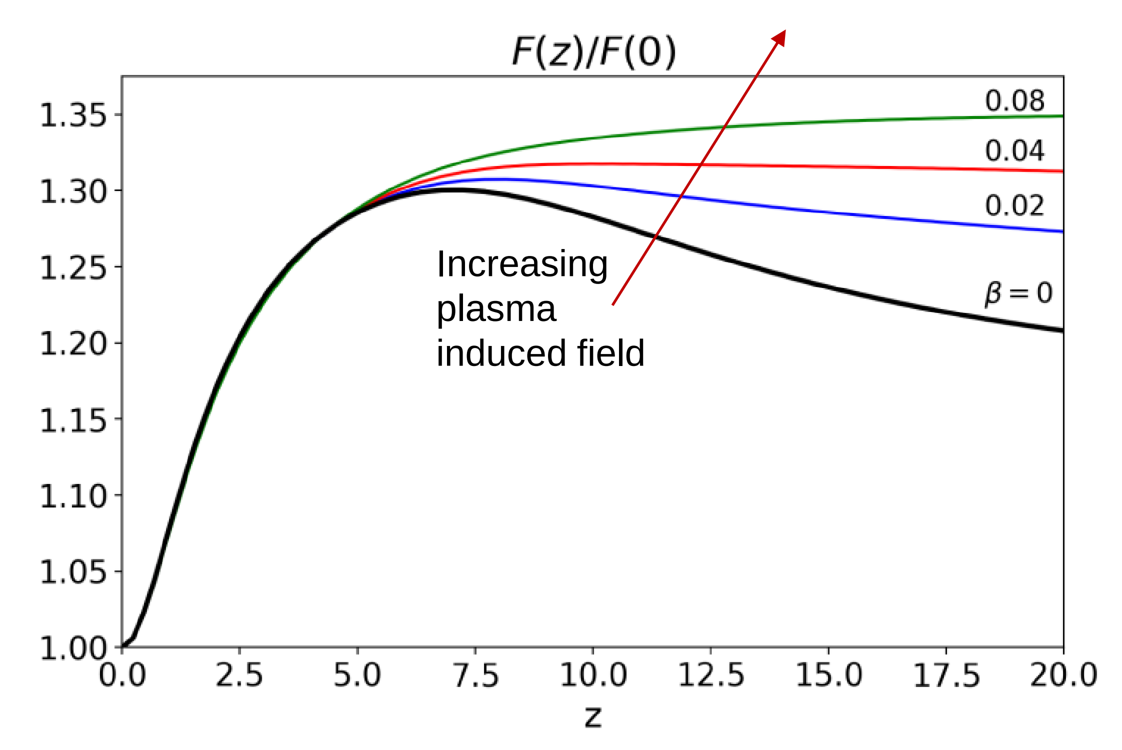

ZARATHUSTRA

Laboratory setup with two ECR plasma sources

- MAT2 thruster is a dual coaxial ECR thruster to experimentally validate the magnetic arch concept for plasma acceleration

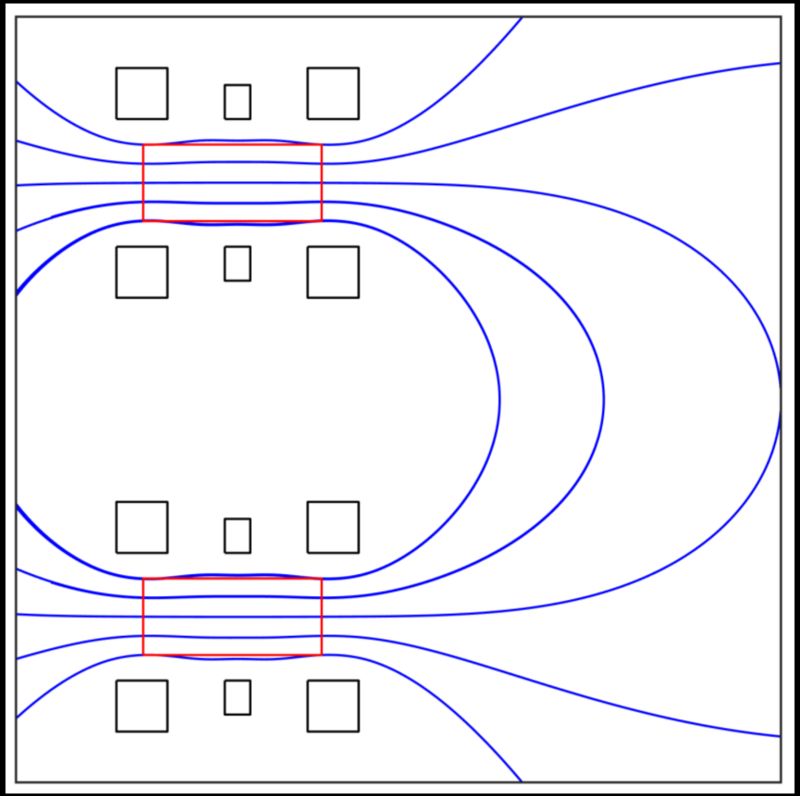

MAT2 Architecture

Electromagnets

Maximum total power per source	1 kW
Maximum magnetic field intensity	900 G
ECR resonance field	875 G
Total number of turns per source	≈ 1200

Ionisation chamber

Length	50 mm
Diameter	30 mm
Material	Non-magnetic Stainless Steel

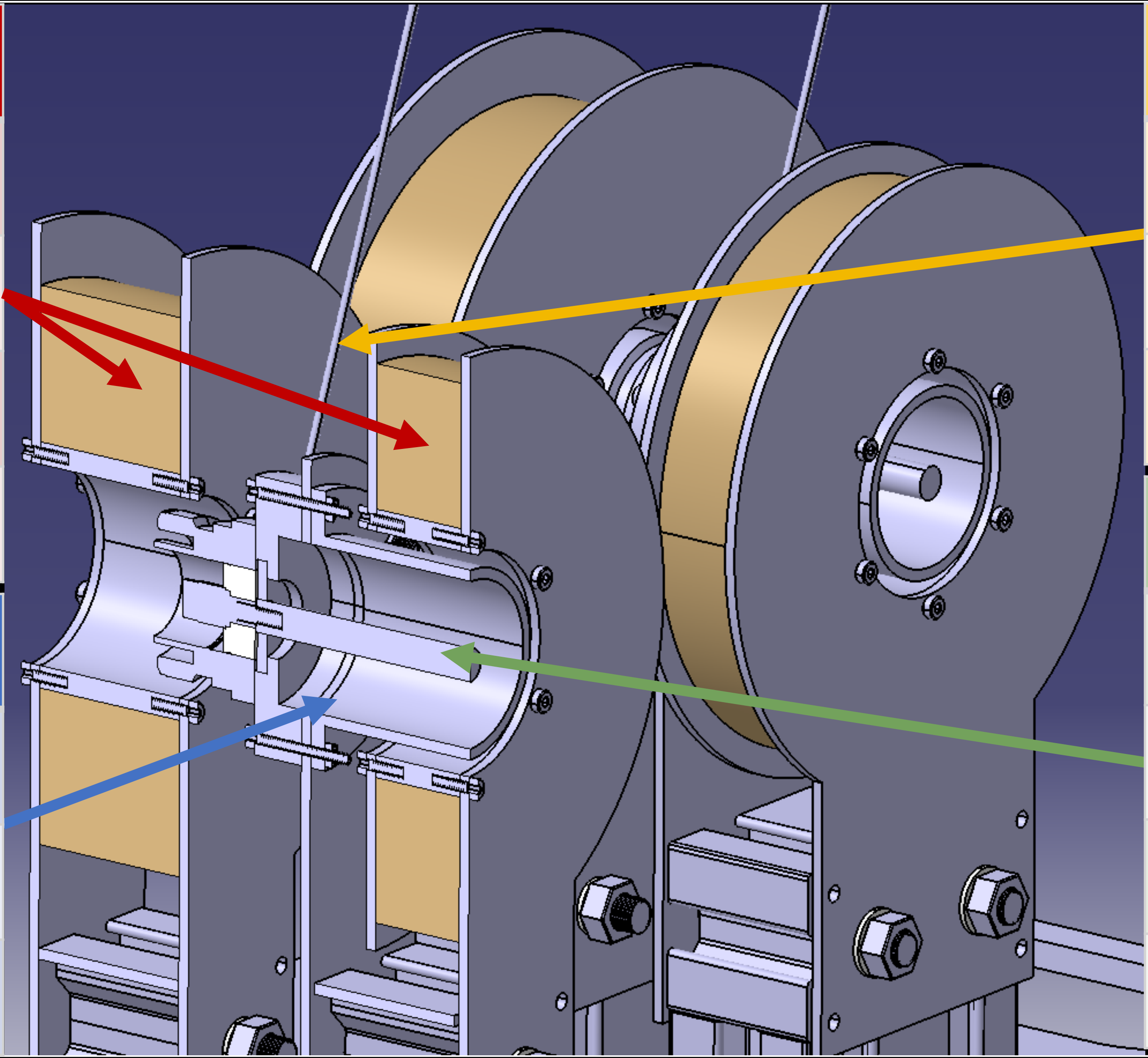

Gas feeding

Gas	Krypton
Ignition mass flow rate	50 sccm
Operation mass flow rate	15 sccm

Inductor

Length	50 mm
Diameter	6 mm
Frequency	2.45 GHz
Power	50 W–500 W

Experimental Setup

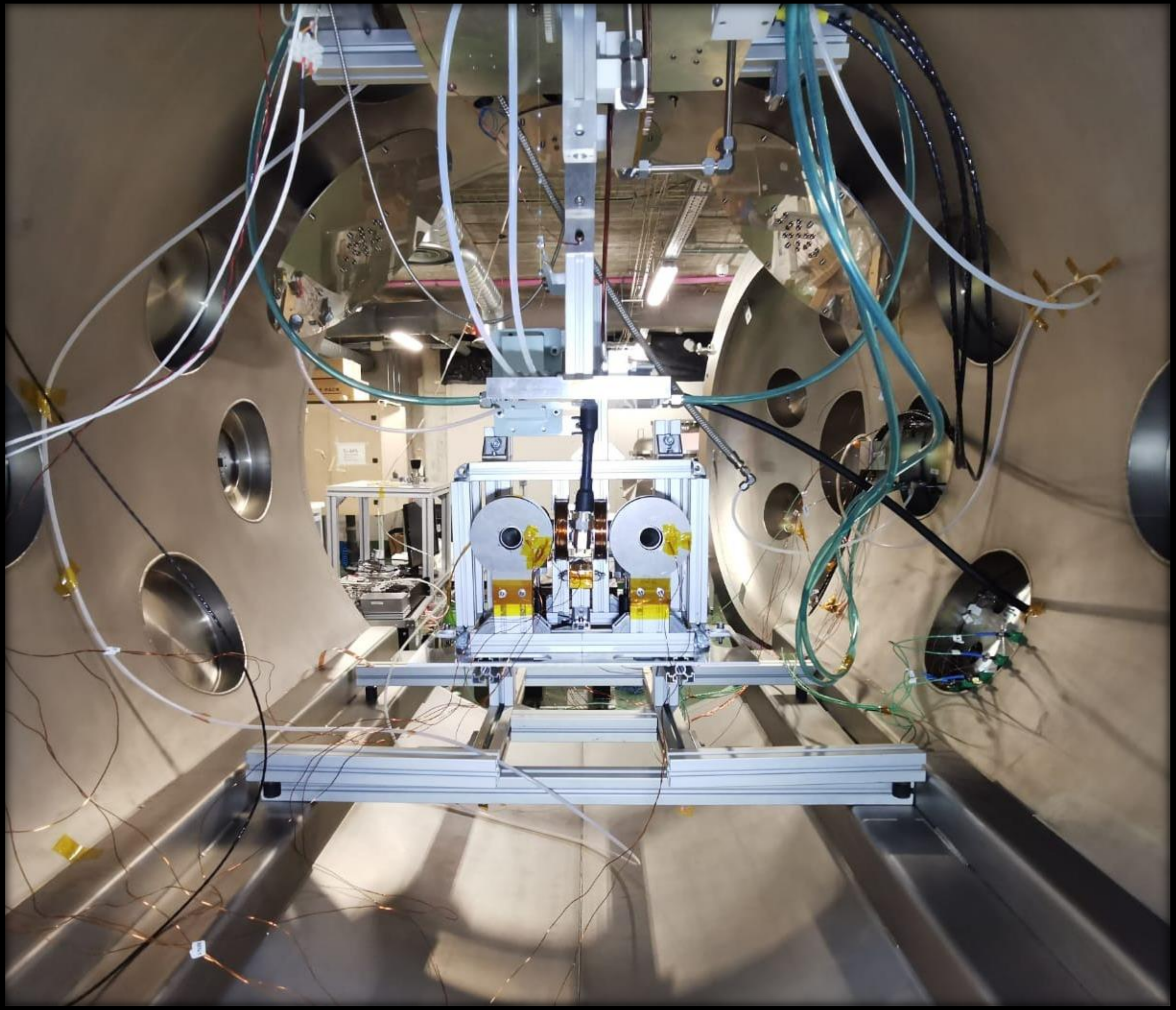

MAT2 Thrutster installed in the EP2 group vacuum chamber

- Technology in use:
  - *Primary pump:* *Leybold **Leyvac LV 80*** $(80\ m^3/h)$
  - *Turbomolecular pumps:* *2 **MAGW2.200iP*** $(2000\ l/s)$
  - *Cryopanels:* *3 Leybold **Leyvac 140 T-V***
  - *Leak dectector:* *Leybold **L300i***

Vacuum chamber characteristics	
Length	$3.5m$
Diameter	$1.5m$
Operational pressure	$2e-5mbar$ at $20sccm$ of Xe
Pumping speed	$> 37000\ l/s$ of Xe

Experimental Setup

- Radial / Polar positioning system used in the vacuum chamber with a Retarded Potential Analyzer (RPA) and two Faraday Cups (FC).

- RPA characteristics: ← This presentation
  - Distance to the thruster: $380mm$
  - Number of holes per grid: 37
  - Ion collection area: $A = 1.86e - 5$ m²
  - Transmission factor: $T = 0.0625$
  - Set of angles: $[-50°, -25°: 5°: 25°, 50°]$
  - $IEDF$, $\overline{E}_i$, $\overline{v}_i$, I_{Tot}

- FC characteristics:
  - Distance to the thruster: $380mm$
  - Set of angles: $[-90°: 90°]$
  - I_{tot}

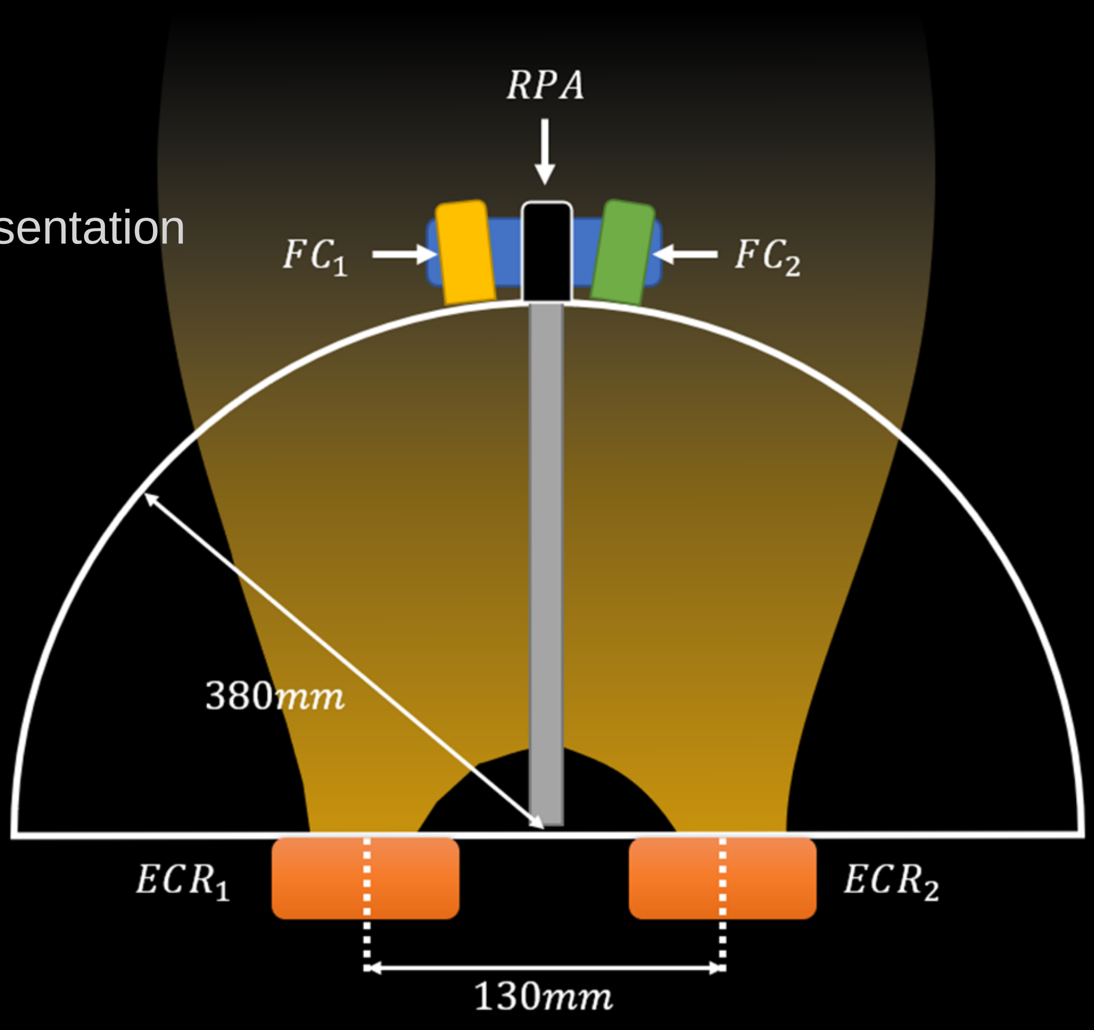

Experimental Setup

- Two magnetic topologies have been characterized.

*Magnetic field with "**MF ARCH**" configuration.*

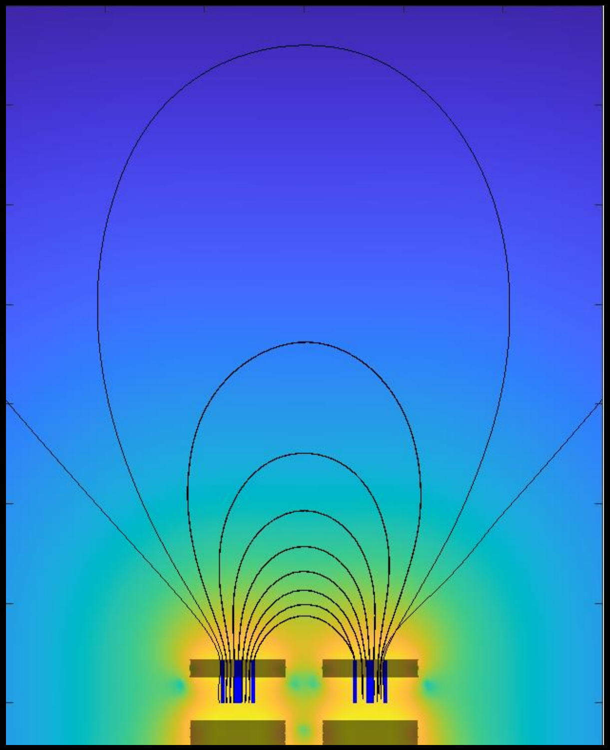

*Magnetic field with "**MF SP**" configuration.*

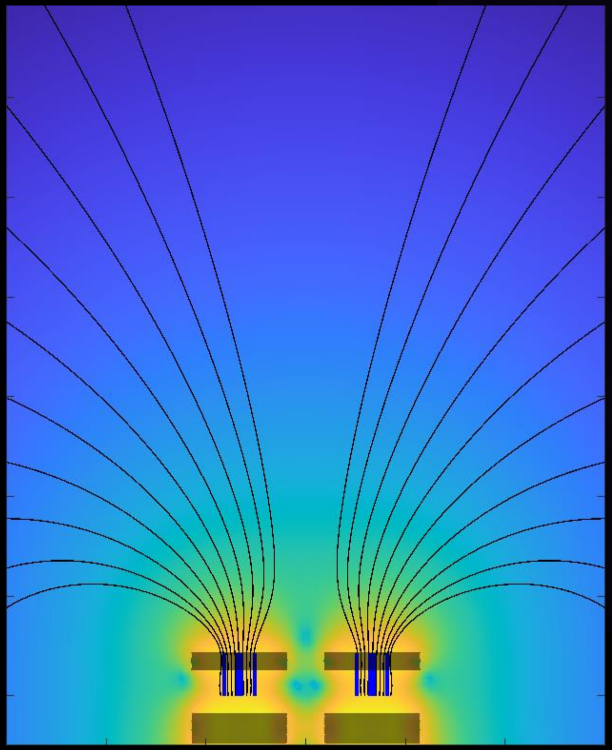

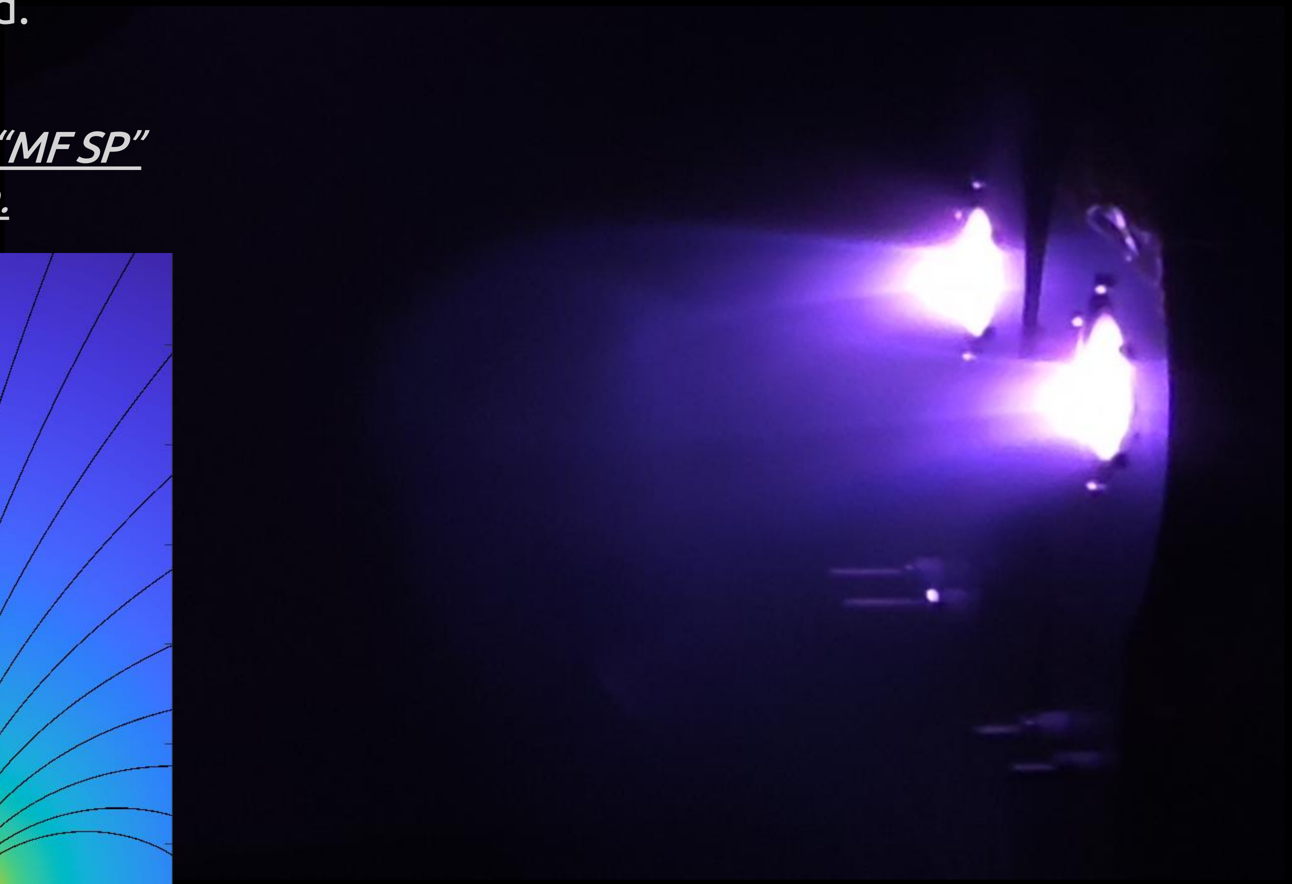

*Thrusters in operation with Krypton in **MF ARCH** configuration.*

Results – Ion Flux

- Ion flux computed with data from the RPA:

$$I_{TOT} = \frac{\int_{E_{min}}^{E_{max}} f(E)\, dE}{A}$$

- MF Arch is seen to generate a single-peaked ion beam, in spite of the closed magnetic lines, validating the concept for plasma acceleration

- MF Reverse: two-peaked ion flux, consistent with the two "deflected" magnetic nozzles.

- MF Off: ion flux flat and one order of magnitude lower (larger area expansion ratio and worse plasma production)

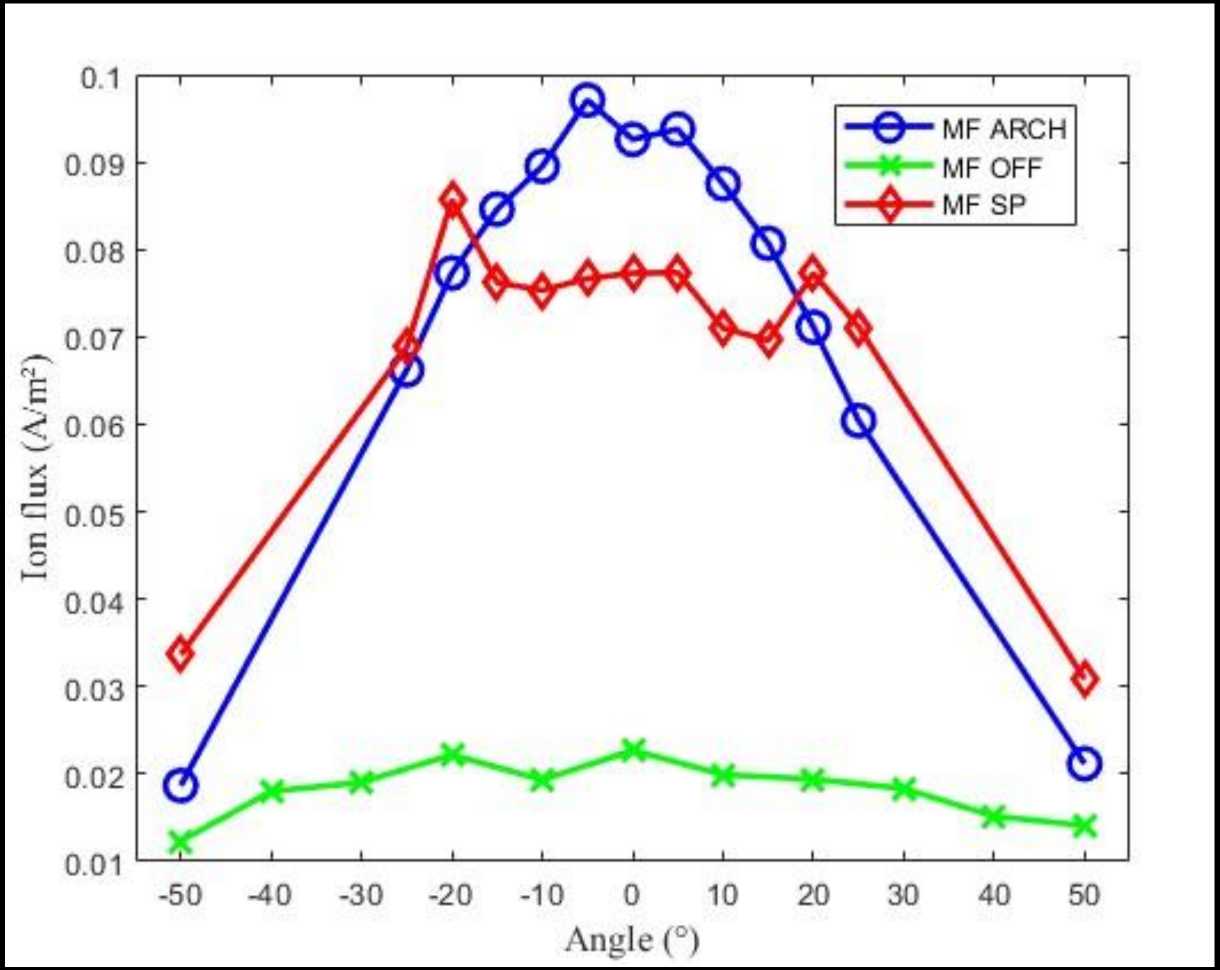

Results – Average Ion Energy and Velocity

- Mean energy computed with data from the RPA:

$$\bar{E}_i = \frac{\int_{E_{min}}^{E_{max}} E\, f(E)\, dE}{\int_{E_{min}}^{E_{max}} f(E)\, dE}$$

- Ion energy depends, at least partially, on area expansion ratio (greater for MF Off)

- Lower energy in MF Arch could be due to
  - Lower area expansion ratio (good, less plume divergence)
  - Small drag contribution due to closed lines
  - Lower overall electron temperature (ion acceleration $\propto T_e$)

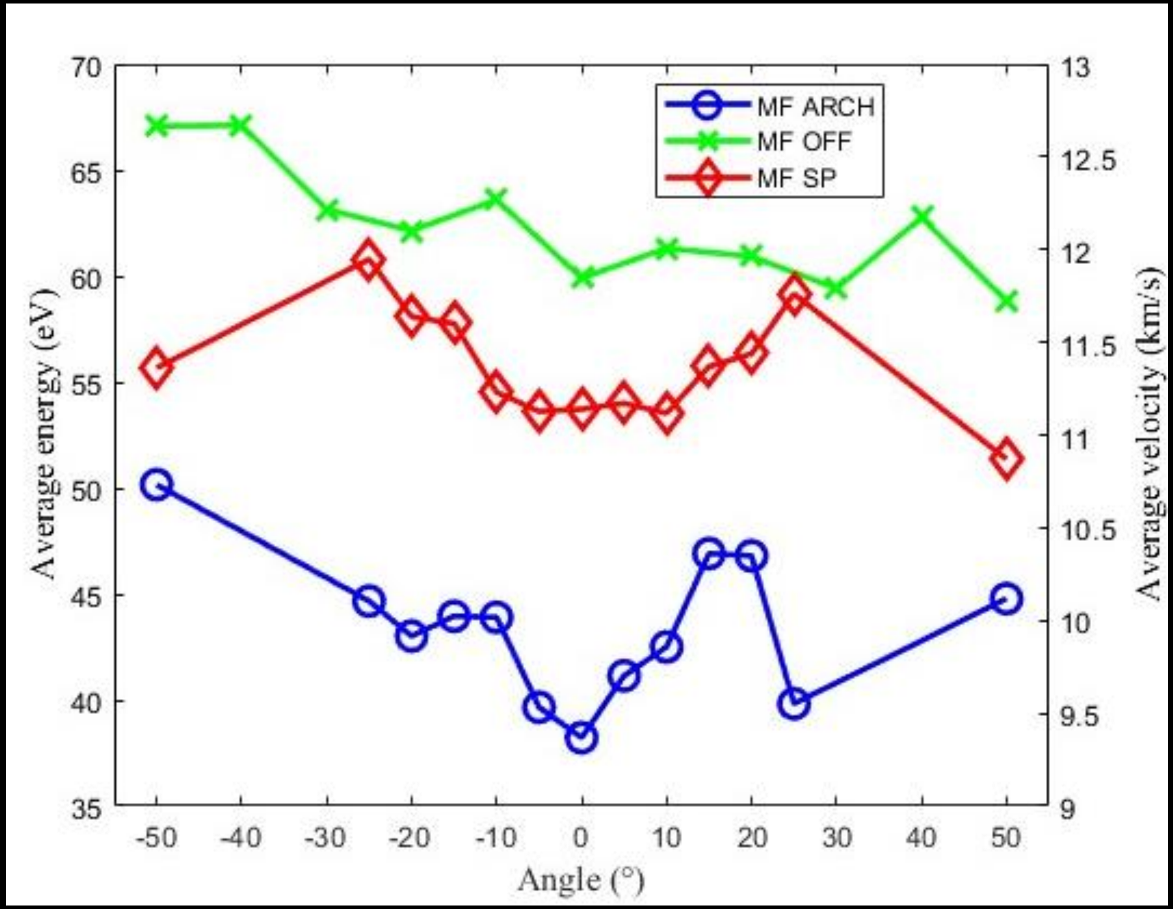

Results – One source Thruster Comparison

- Lower plume divergence and lower ion energy than single source magnetic nozzle
- Results support first two hypotheses (lower area expansion ratio and effect of drag contribution due to closed lines)

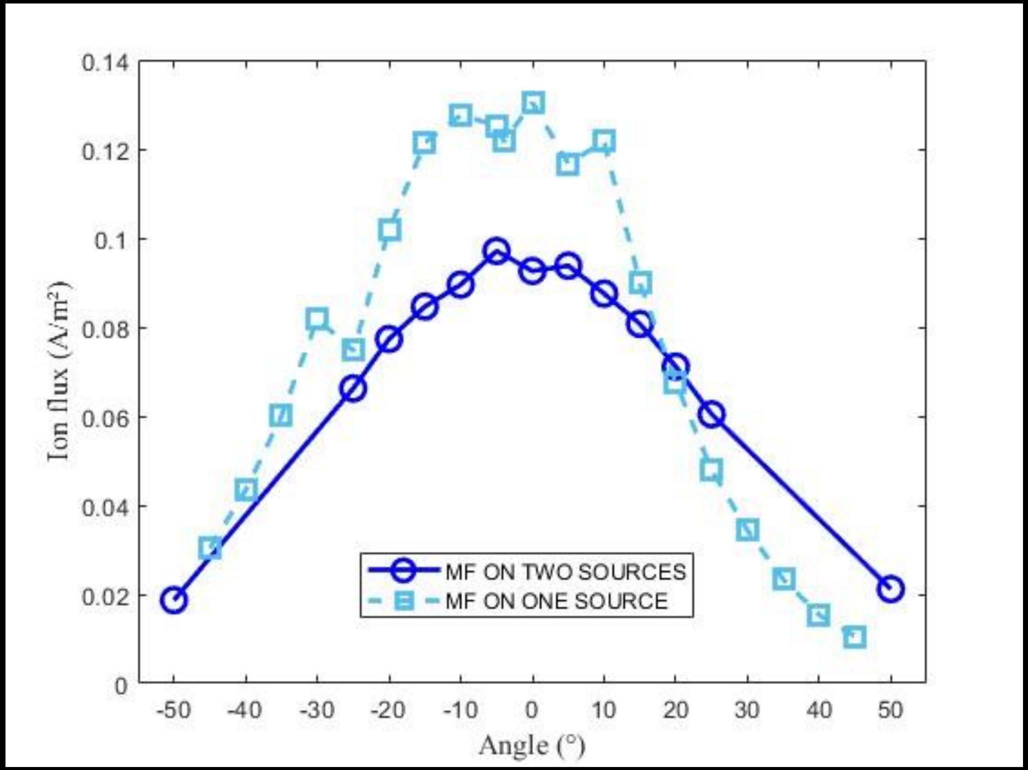

Comparison of the ion flux in between one and two sources.

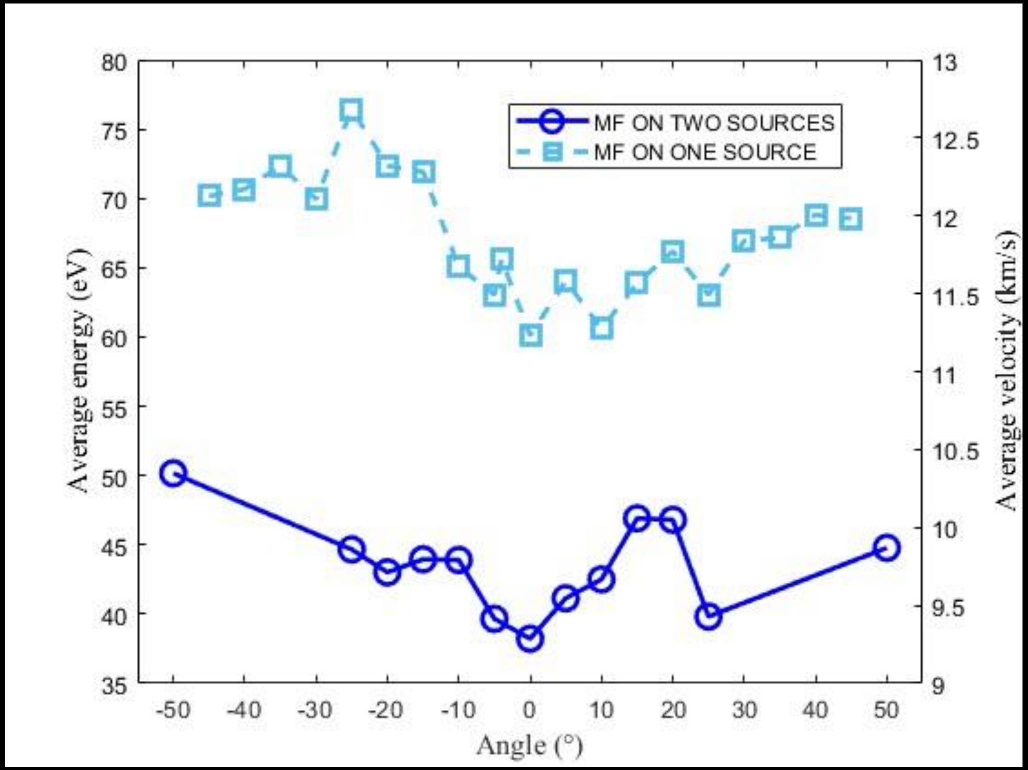

Comparison of the average energy and velocity in between one and two sources.

Conclusions

- A (2D planar) two fluid model and an experimental setup with two ECR sources have demonstrated the magnetic arch for plasma acceleration
- Relevant for tandems of electrodeless plasma thrusters (to cancel magnetic dipole) and for new geometries (C-shaped thruster)
- Free plasma beam forms in spite of closed lines

- Model shows the crucial role of the plasma-induced magnetic field to stretch the field lines and increase magnetic thrust.
In contrast, in an axisymmetric magnetic nozzle, induced field plays a secondary role

- Experiments show single-peaked ion current profile, in contrast with same-polarity configuration. Lower ion energy is partially justified by the lower plume divergence in the magnetic arch configuration, and due to the small drag contribution of closed lines

[First simulation results just accepted on PSST: DOI 10.1088/1361-6595/acd476]

Acknowledgments

This project has received funding from the European Research Council (ERC) under the European Union's Horizon 2020 research and innovation programme (grant agreement No 950466)

Thank you!

mario.merino@uc3m.es

ZARATHUSTRA

MAT2 Architecture

- 2.45 GHz tunable (± 50 MHz) solid state microwave generator (Muegge MR1000D-200ML).
- 7-16 DIN coaxial 2.45 GHz graded feedthrough (Allectra 242-7_16-K50).
- Coaxial $2.45 GHz$ graded all females three ways splitter (Microlab D2-16FD).
- M3 termination 7-16 DIN panel crimp (Telegartener J01121A0721).
- Elements connected with coaxial cables:
  - LMR-600-FR coaxial cables
  - TC-600-716M-X coaxial connectors.